12^{th} International Conference on Fracture Mechanics of Concrete and Concrete Structures
FraMCoS-12
B.L.A. Pichler, Ch. Hellmich, P. Preinstorfer (Eds)

https://doi.org/10.21012/FC12.1290
MS08-2:2

WOOD CONSTITUTIVE LAW IMPLEMENTATION AND PARAMETER CALIBRATION USING BAYESIAN INVERSION FOR FINITE-ELEMENT MODELLING

M. DELAGE[*,†], D. SCANTAMBURLO[†], G. JACOT-DESCOMBES[*] AND S. COMMEND[*,‡]

[*] GeoMod ingénieurs conseils SA
Epinettes 32, 1007 Lausanne, Switzerland
e-mail: mdelage@geomod.ch, www.geomod.ch

[†]MONOD – PIGUET + ASSOCIES Ingénieurs Conseils SA
Avenue de Cour 32, 1007 Lausanne, Switzerland
www.mpaic.com

[‡]School of Engineering and Architecture, HES-SO
University of Applied Sciences Western Switzerland
1700 Fribourg, Switzerland
www.hes-so.ch

Key words: Wood, Continuum damage mechanics, Orthotropy, Numerical finite element simulation, Bayesian inversion

Abstract. This paper presents three-dimensional finite element simulations of wooden structures using metal connections that employ an elastic-plastic damage model in order to simulate the nonlinear behaviour of wood. The wood constitutive law relies upon orthotropic material parameters, associated plasticity and continuum damage mechanics (CDM) to take into account the following properties of wood : anisotropy, brittle failure in tension, plasticity and ductile failure in compression. The model used in this paper is implemented as a user subroutine of the finite element software ZSoil. Experimental uniaxial compression tests on small wood samples are utilized to conduct a calibration of the material parameters. This calibration is performed by generating a Polynomial Chaos Expansion surrogate model of the true finite-element model, which is then used for a Bayesian inversion on the experimental data from tests on small wood samples. The constitutive model with the calibrated material parameters is then used to numerically reproduce experimental tests on wooden structures. The results demonstrate the model's capability to reasonably approximate the nonlinear behaviour of wood along with its interaction with metal connections, opening up interesting prospects for engineers to better understand and optimise wooden structures.

1 INTRODUCTION

Timber is an widely used material in the construction field thanks to its interesting mechanical properties. In addition to that, using structural wood in constructions allows to decrease their carbon footprints which makes it more and more beneficial to use wood even for non-traditional wooden structures such as multi-storey building. Still, modelling those type of structures remains challenging due to the non-linear and anisotropic behaviour of wood coupled with the wood-steel interaction at joints.

Numerical simulations and especially finite-element modelling allow to reproduce the me-

chanical behaviour of materials when using appropriate constitutive laws. That implies to take into account the linear and nonlinear anisotropy of wood as well as its post-elastic plasticity and brittle failure. Several models have been developed to approach those characteristics including several criteria to trigger the nonlinear behaviour.

In this paper, a constitutive 3D model for wood is developed using a Hoffman criterion for plasticity and a Sandhaas criteria to determine failure modes. The model is then calibrated on experimental data and tested on reinforced beams.

2 CONSTITUTIVE ASPECTS

Wood is represented as an orthotropic material with three principal directions defined with respect to grain direction and growth rings. Fig. 1 shows these three directions: longitudinal (L), radial (R) and tangential (T).

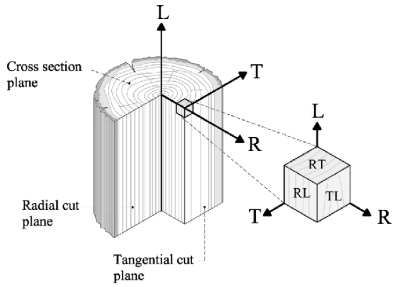

Figure 1: Definition of material directions in wood matrix

2.1 Stress strain relationship

The stress strain relationship is governed by the fundamental Hooke equation (Eq. 1):

$$\bar{\boldsymbol{\sigma}} = \mathbf{D_0} : \boldsymbol{\varepsilon}^e \tag{1}$$

With $\mathbf{D_0}$ the orthotropic elastic stiffness tensor and $\boldsymbol{\varepsilon}^e$ the elastic strain tensor. The constitutive law employs Continuum Damage Mechanics (CDM) to model cracks in the material matrix [1, 2]. Thus, the Cauchy stress tensor $\boldsymbol{\sigma}$ is related to the effective stress tensor $\bar{\boldsymbol{\sigma}}$ by means of a damage tensor $\mathbf{M(d)}$ (Eq. 2) [3, 4]:

$$\boldsymbol{\sigma} = \mathbf{M(d)} : \bar{\boldsymbol{\sigma}} \tag{2}$$

2.2 Plasticity algorithm

Following the work of Sirumbal-Zapata [2], the plasticity is applied solely in compression. Thus, the effective tensor is separated as follows (Eq 3) by a spectral decomposition:

$$\bar{\boldsymbol{\sigma}}^+ = \sum_{i=1}^{3} \langle \bar{\sigma}_i \rangle \mathbf{p}_i \otimes \mathbf{p}_i \quad ; \quad \bar{\boldsymbol{\sigma}}^- = \bar{\boldsymbol{\sigma}} - \bar{\boldsymbol{\sigma}}^+ \tag{3}$$

Where $\langle \bar{\sigma}_i \rangle$ are the positive part of each eigenvalues and $\mathbf{p}_i$ the related eigenvectors.

The plasticity is triggered by Hoffman yield criterion (Eq. 4) [5] applied on the compressive effective stress:

$$f_p = \frac{1}{2}\bar{\boldsymbol{\sigma}}^{-\intercal}\boldsymbol{P}\bar{\boldsymbol{\sigma}}^- + \bar{\boldsymbol{\sigma}}^{-\intercal}\boldsymbol{q}(k) - \bar{\sigma}_y^2(k) \geq 0 \tag{4}$$

Where the reference yield stress is defined as (Eq. 5), k being the isotropic hardening variable:

$$\bar{\sigma}_y(k) = \bar{\sigma}_{y,0}(k) + hk \quad ; \quad \bar{\sigma}_{y,0}(k) = 1 \tag{5}$$

The associated plastic flow rule is given as :

$$\begin{aligned} \dot{\boldsymbol{\varepsilon}}^p &= \dot{\lambda}\boldsymbol{n}(\bar{\boldsymbol{\sigma}}^-, k) \quad \text{with :} \\ \boldsymbol{n} &= \left(\frac{\partial f_p(\bar{\boldsymbol{\sigma}}^-, k)}{\partial \bar{\boldsymbol{\sigma}}^-}\right)^{\intercal} = \boldsymbol{P}\bar{\boldsymbol{\sigma}}^- + \boldsymbol{q}(k) \\ \dot{k} &= \dot{\lambda}\sqrt{\boldsymbol{n}^{\intercal}\mathrm{diag}[1,1,1,{}^1\!/_2,{}^1\!/_2,{}^1\!/_2]\boldsymbol{n}} \end{aligned} \tag{6}$$

2.3 Damage model

The damage is modelled using CDM. The model takes into account four different failure modes : three modes in tension in all three main directions and one mode in compression in the direction of the fibres. For each failure mode, the failure criterion is evaluated only if the related stress component σ_{ii} $(i = L, R, T)$ is positive for a tensile mode and negative for a compressive mode.The following Sandhaas damage criteria [1] are employed :

$$\begin{aligned} F_{L,c} &= -\frac{\bar{\sigma}_{LL}}{f_L^t} \geq 1 \\ F_{L,t} &= \frac{\bar{\sigma}_{LL}}{f_L^t} \geq 1 \\ F_{R,t} &= \left(\frac{\bar{\sigma}_{RR}}{f_R^t}\right)^2 + \left(\frac{\bar{\sigma}_{LT}}{f_{LR}^s}\right)^2 + \left(\frac{\bar{\sigma}_{RT}}{f_{RT}^s}\right)^2 \geq 1 \\ F_{T,t} &= \left(\frac{\bar{\sigma}_{TT}}{f_T^t}\right)^2 + \left(\frac{\bar{\sigma}_{LT}}{f_{LT}^s}\right)^2 + \left(\frac{\bar{\sigma}_{RT}}{f_{RT}^s}\right)^2 \geq 1 \end{aligned} \tag{7}$$

The tensile damage evolution function [6] for $i = L, R, T$ is given as :

$$d_{i,t} = 1 - \frac{1}{F_{i,t}} \exp\left((1 - F_{i,t})\frac{L_c f_i^{t2}}{E_i G_{f,i}}\right) \quad (8)$$

Where L_c is the characteristic length of the element and is defined as the cubic root of the element volume : $L_c = \sqrt[3]{V_e}$ [7].

The compressive damage function is expressed as follows:

$$d_{Lc} = 1 - \frac{1}{F_{L,c}}(1 - A) - A\exp\left(B(1 - F_{L,c})\right) \quad (9)$$

Where parameters A and B are calibrated thanks to material tests. The initial value for all damage variable is null. To ensure the damage connot decrease in the material, the damage variable at the step $n + 1$ is set as follows :

$$d_{i,c/t}^{n+1} = max(d_{i,c/t}, d_{i,c/t}^{n}) \quad (10)$$

The damage matrix is defined as in Eq. 11 where $d_i = d_{i,t}$ if $\sigma_{ii} \geq 0$ and $d_i = d_{i,c}$ otherwise.

$$\begin{aligned}\mathbf{M}(\mathbf{d}) = \text{diag}([&(1 - d_L),\ (1 - d_R),\ (1 - d_T),\\ &\sqrt{(1 - d_R)(1 - d_T)},\\ &\sqrt{(1 - d_L)(1 - d_T)},\\ &\sqrt{(1 - d_L)(1 - d_R)}\,])\end{aligned} \quad (11)$$

2.4 Viscous regularization

To improve the convergence of the algorithm, a viscous regularization is applied, following the method proposed by Duvaut and Lions [8] and discretized :

$$\begin{aligned}\dot{d}^v &= \frac{1}{\eta}(d - d^v)\\ d_{n+1}^v &= \frac{\eta}{\eta + \Delta t} d_n^v + \frac{\Delta t}{\eta + \Delta t} d_{n+1}\end{aligned} \quad (12)$$

3 NUMERICAL IMPLEMENTATION

The constitutive law is implemented in a user-defined subroutine on the finite element software ZSoil [9]. The input of the algorithm is an increment of strain along with the values from previous step.

The algorithm first calculates a trial effective stress (Eq. 1) that is decomposed (Eq. 3) into a tensile and a compressive part. The compressive trial effective stress is then substituted in the yield function (Eq. 4) and a Newton-Raphson algorithm calculates the plastic increment if the plastic criterion is met. This allows to determine the effective stress.

The CDM algorithm takes as an input the new effective stress and evaluates the failure criteria compatible with the stress state (Eq. 8). The new damage variables can then be calculated (Eq. 8 and 9) and regularized (Eq. 12). Finally, the damage tensor (Eq. 11) and therefore the Cauchy stress tensor (Eq. 2) can be evaluated.

4 MODEL CALIBRATION

The constitutive law is tested and calibrated on experimental tests from Karagiannis et al. [10].

4.1 Parameter calibrations

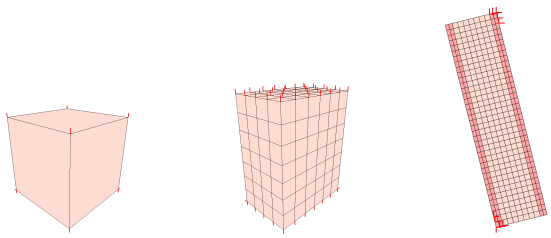

(a) (b) (c)

Figure 2: Finite-element wood samples loaded in compression in three different directions (a) Loading parallel to the fibre (b) Loading perpendicular to the fiber (c) Shear test

The experimental tests [10] are performed on three parallelepipedal wood samples to characterize the behaviour in compression and in shear. These three tests are named in the rest of the paper the characterization tests. The samples are modelled on the finite-element software ZSoil. Fig. 2a is a compression in the direction of the fibres (L), Fig. 2b is a compression in

the direction perpendicular to the fibres (R) and Fig. 2c is a shear test.

The model parameters are calibrated by a Bayesian inversion using the software UQLab [11]. A Monte-Carlo sampling of the parameters is performed, giving 300 sets of parameters that are tested on the three characterization tests. The statistical distribution of each parameter is uniform, with at least a thirty percent variation around the mean value. The quantities of interest for each test are four stress/strain states distributed on the loading path. The stress and strain states are analytically estimated through the force and displacements results on the load application surfaces of the finite element model in order to ensure the coherence between the numerical results and the experimental ones.

A Polynomial Chaos Expansion (PCE) is built on this sampling and numerical outputs, allowing for the use of Bayesian inversion to calibrate the material parameters thanks to the surrogate model. The experimental reference points corresponding to each quantity of interest are indicated on Fig 3,4,5. The calibration resulted in the following set of material parameters for the spruce used in the experimental tests:

Table 1: Calibrated material parameters' value

$E_L = 2157$	$E_R = 164$	$E_T = 164$	MPa
$G_{LR} = 221$	$G_{RT} = 54$	$G_{TL} = 221$	MPa
$\nu_{LR} = 0.4$	$\nu_{RT} = 0.5$	$\nu_{TL} = 0.03$	-
$f_L^+ = 24$	$f_R^+ = 0.5$	$f_T^+ = 0.5$	MPa
$f_L^- = 39$	$f_R^- = 1.6$	$f_T^- = 1.6$	MPa
$f_{LR} = 6.1$	$f_{RT} = 0.6$	$f_{TL} = 6.1$	MPa
$G_{f,L} = 77$	$G_{f,R} = 8$	$G_{f,T} = 8$	$^{\mathrm{N}}/_{\mathrm{mm}}$
	$h = 1.6$		-
	$A = 0.3$		-
	$B = 0.8$		-

The finite element simulations of the characterization tests with the calibrated parameters for the wood constitutive law resulted in the stress-strain curves shown below. The numerical results are compared with the upper and lower boundaries of the experimental results. Fig. 3, Fig. 4 and Fig. 5 are related respectively to Fig. 2a, Fig. 2b and Fig. 2c.

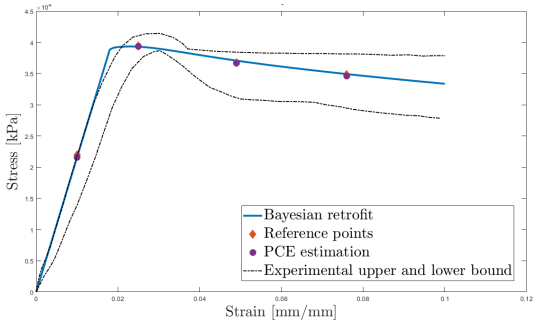

Figure 3: Compression stress-strain relationship for spruce parallel to the grain

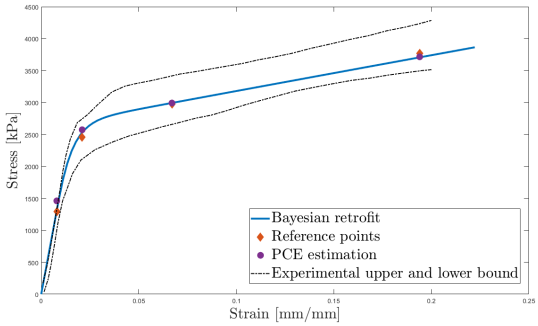

Figure 4: Compression stress-strain relationship for spruce perpendicular to the grain

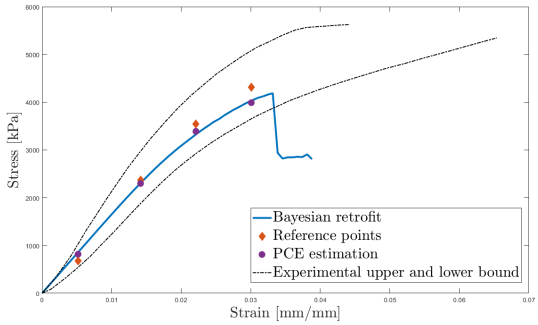

Figure 5: Shear stress-strain relationship for spruce

4.2 Calibration validation

The model and the calibrated parameters are tested on dowel-embedment tests from Karagiannis et al. paper [10]. Fig. 6 shows the fi-

nite element mesh reproducing the experimental tests. Fig. 7a is a vertical loading of the dowel in compression with the fibres along the vertical directions and Fig. 7b with the fibres in the horizontal direction. The results plotted on Fig. 7 show good agreement with the experimental results.

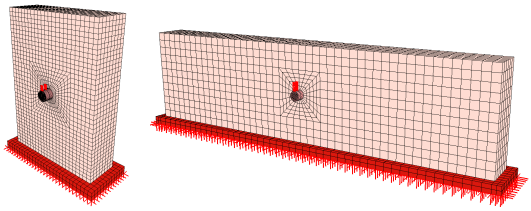

(a) (b)

Figure 6: Finite element mesh for the dowel embedment test

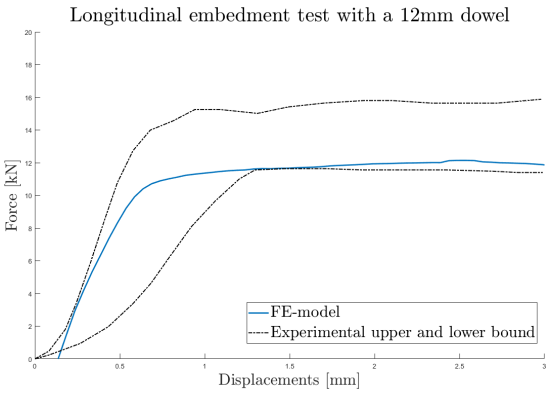

(a)

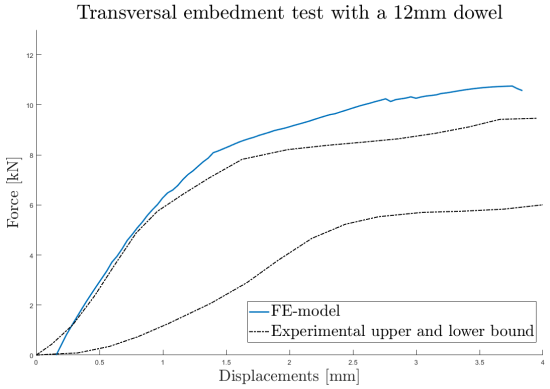

(b)

Figure 7: Numerical results of the dowel-embedment tests compared to the experimental results

5 EXPERIMENTAL TEST ON WOODEN BEAMS WITH HOLES

The constitutive model is used to numerically predict the behaviour of wooden beams with holes.

5.1 Geometry

The beams are 7 meters long with a 240x280mm section (bxh) (see Fig. 8). The test is four points bending of a simply supported beam. The vertical loading is displacement-controlled.

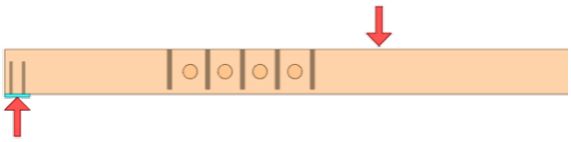

Figure 8: Reinforced beam with holes

The beams are internally reinforced with threaded rods. Two reinforcements are tested, a first case with five rods perdipendicular to the grain (Fig. 9a) and a second case with five rods with a 45° inclination to fibre direction (Fig. 9b).

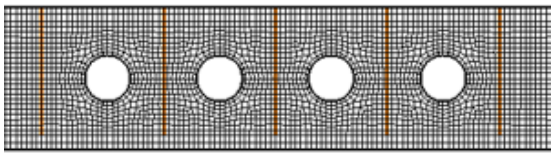

(a)

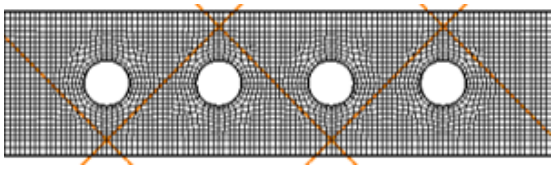

(b)

Figure 9: Reinforcements around the holes with threaded steel rods

5.2 Materials

The GLT beams are assigned spruce glulam GL24h material properties. The elastic stiffness properties and failure strength are attributed following the characteristic values for GL24h. The

Poisson ratios ν_{ij}, the fracture energies $G_{f,i}$, the hardening modulus h and the nonlinear parameters A and B for glulam spruce are determined thanks to the calibration tests detailed in previous sections. The steel rods are modelled as an elastic material with $E = 210\text{GPa}$ and $\nu = 0.3$. The glue connecting the rods to the wood is not modelled and is assumed to ensure a fully bonded interface.

5.3 Results

The finite element simulations failure maps are similar for both types of reinforcement. The damage localization for reinforcements perpendicular to the fibres is shown on Fig. 10. The failure appears around the holes at a 45° angle with the vertical axis corresponding to a shear dominant loading of a wooden beam [12].

The ultimate vertical load for the beam without reinforcement and for the two types of reinforcements with rods are listed in Tab. 2. The indicated force is the load for the half beam.

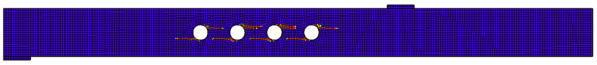

Figure 10: Failure of wood for a beam reinforced with vertical steel rods

Table 2: Ultimate load of the four-points bending tests

	F_y [kN]
Unreinforced beam	45
Vertical reinforcements	68
Inclinated reinforcements	70

6 CONCLUSIONS

The implemented constitutive law and its calibration has shown good results to reproduce dowel-embedment tests. The constitutive law has also been used to model wooden beams giving encouraging qualitative results that are to be supported with experimental data.

REFERENCES

[1] Carmen Sandhaas, Jan-Willem van de Kuilen, and H. Blass. Constitutive model for wood based on continuum damage mechanics. *World Conference on Timber Engineering 2012, WCTE 2012*, 1, 01 2012.

[2] Luis F. Sirumbal-Zapata, Christian Málaga-Chuquitaype, and Ahmed Y. Elghazouli. A three-dimensional plasticity-damage constitutive model for timber under cyclic loads. *Computers & Structures*, 195:47–63, 2018.

[3] A. Matzenmiller, J. Lubliner, and R.L. Taylor. A constitutive model for anisotropic damage in fiber-composites. *Mechanics of Materials*, 20(2):125–152, 1995.

[4] J.C. Simo and J.W. Ju. Strain- and stress-based continuum damage models—i. formulation. *International Journal of Solids and Structures*, 23(7):821–840, 1987.

[5] Oscar Hoffman. The brittle strength of orthotropic materials. *Journal of Composite Materials*, 1(2):200–206, 1967.

[6] Mingqian Wang, Xiaobin Song, and Xianglin Gu. Three-dimensional combined elastic-plastic and damage model for nonlinear analysis of wood. *Journal of Structural Engineering*, 144, 08 2018.

[7] Zdenek Bazant and Byung Oh. Crack band theory for fracture of concrete. *Matériaux et Constructions*, 16:155–177, 05 1983.

[8] G. Duvaut and J. L. Lions. Inequalities in mechanics and physics. *Grundlehren Der Mathematischen Wissenschaften*, 1976.

[9] ZSOIL 2023. *A Windows-Based Tool offering a unified approach to numerical simulation of soil and rock mechanics, above & underground structures, excavations, soil-structure interaction and*

underground flow, including dynamics, thermal and moisture migration analysis. GeoDev SARL.

[10] V. Karagiannis, C. Málaga-Chuquitaype, and A.Y. Elghazouli. Modified foundation modelling of dowel embedment in glulam connections. *Construction and Building Materials*, 102:1168–1179, 2016. SHATIS 2013 : Research on Timber Materials and Structures.

[11] Stefano Marelli and Bruno Sudret. *UQLab: A Framework for Uncertainty Quantification in Matlab*, pages 2554–2563.

[12] Julia Dröscher, Manfred Augustin, and Gerhard Schickhofer. Comparison of verification and reinforcement concepts for timber beams with large round holes. 08 2016.